Antiferromagnetic properties of DMCTTF salts

1989 J. Phys.: Condens. Matter 1 4971

(http://iopscience.iop.org/0953-8984/1/30/010)

J. Phys.: Condens. Matter 1 (1989) 4971–4984. Printed in the UK

Antiferromagnetic properties of DMCTTF salts

P Vaca†‡, C Coulon†, L Ducasse§, T Granier‖, B Gallois‖, J M Fabre¶ and A K Gouasmia¶

† Centre de Recherche Paul Pascal, Université de Bordeaux I, 33405 Talence Cedex, France

§ Laboratoire de Physico-Chimie Théorique, Université de Bordeaux I, 33405 Talence Cedex, France

‖ Laboratoire de Cristallographie, Université de Bordeaux I, 33405 Talence Cedex, France

¶ Laboratoire de Chimie Structurale Organique, 33060 Montpellier Cedex, France

Received 29 November 1988

Abstract. A new series of salts, the $(DMCTTF)_2X$, has been recently synthesised. These compounds have already been characterised through electrical conductivity and ESR measurements. We summarise this study and present additional results for sulphur compounds with tetrahedral anions. New crystallographic data, transfer-integral calculations and electronic properties in the paramagnetic state are presented. These compounds are characterised by the presence of two organic layers in the unit cell. Moreover, an antiferromagnetic ordering is found for both layers. Thus, we also describe antiferromagnetic resonance data obtained with an X-band spectrometer below the Néel temperature. Finally, we employ these results in discussing the interactions relevant for AF ordering. In particular, we analyse the magnetic anisotropy and the role of the inter-layer interactions.

1. Introduction

In a previous paper (Vaca *et al* 1988), hereafter called paper A, the physical properties of a new series of organic conductors, the $(DMCTTF)_2X$ salts have been described. These radical cation salts can be prepared with the same 2:1 stoichiometry using various diamagnetic anions such as PF_6^-, AsF_6^-, BF_4^-, ClO_4^-, ReO_4^- (Giral *et al* 1986).

A wide variety of physical properties has been found in the series. Among these properties is the occurrence of a larger unit cell containing two organic layers with tetrahedral anions. In the case of sulphur compounds, the influence of the size of the anion has been discussed and two distinct phases with different structural organisations, labelled α and β, have been found.

In this paper we describe these compounds in more detail. A summary of their physical properties in the paramagnetic phase is first given. We then describe the antiferromagnetic phase through antiferromagnetic resonance (AFMR) measurements. Transfer-integral calculations are reported, and finally a detailed discussion of the results is given.

‡ Present address: Department of Physics, Ohio State University, 174 West 18th Avenue, Columbus, OH 43210-1106, USA.

0953-8984/89/304971 + 14 $02.50

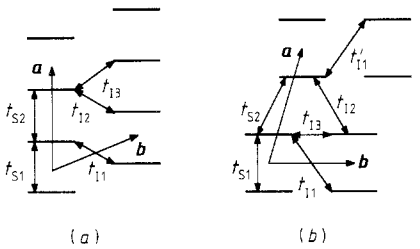

Figure 1. Structural organisation of the organic layers (schematic) (*a*) layers of type I; (*b*) layers of type II. The definition of the different transfer integrals is also given.

2. Physical properties in the paramagnetic phase

2.1. Structural properties

$(DMCTTF)_2X$ salts exhibit various structural organisations depending on the anion size and geometry (A). As far as tetrahedral anions are concerned, two crystalline phases are found. To illustrate this property, $(DMCTTF)_2ClO_4$ is a representative example, since both phases have been found in the same batch of samples. Following the notation of paper A, the first one is called the α-phase. It is isomorphic to $(DMCTTF)_2BF_4$. The second one, the β-phase, is isomorphic to the ReO_4 salt.

The α- and β-salts crystallise with monoclinic and triclinic symmetry respectively. Both phases are characterised by the fact that the crystals contain two different DMCTTF layers. In the α-phase the different layers are symmetry-related through a two-fold screw axis parallel to the ***b*** monoclinic axis. This implies that the structure of both layers is identical. This is no longer the case for β-salts, where the two layers are not symmetry-related. In this case, not only are the stacking axes of the DMCTTF molecules different but also their organisation in the layers. One layer (labelled I) is weakly dimerised. The other (type II) presents a much more important dimerisation. Figures 1(*a*) and 1(*b*) give the projections of both layers along the long molecular axis. Both layers are of type II in the α-phase.

It is important to note that layers of type II are not identical in α- and β-phases. This is, for example, illustrated by the conformation of the DMCTTF molecules. Differences are found in the relative positions of the carbon atoms located at the end of the outer ring. A boat-like conformation is found for the α-phase, as for the layers of type I of the β-phase. On the other hand, the layer II of the β-phase presents a chair-like conformation. Other differences are found in the relative positions of the molecules. This explains the different magnitude of some transfer integrals between neighbouring molecules (see § 4). Other details on these structures will be given separately (Granier and Gallois 1989).

2.2. Electronic properties

Various electronic properties are also found for the series. The electrical conductivity of α-salts is weak, with a semiconducting behaviour and a large gap even at room temperature (about 2500 K). For β-salts, the conductivity is dominated by layers of type I: a higher absolute value is measured at room temperature and a broad minimum of resistivity is found at $T_\rho \simeq 200$–300 K.

The magnetic susceptibility of α-salts is characteristic of a spin lattice with a maximum at $T \simeq 65$ K. A superposition of the behaviours of layers of type I and II is found for β-compounds.

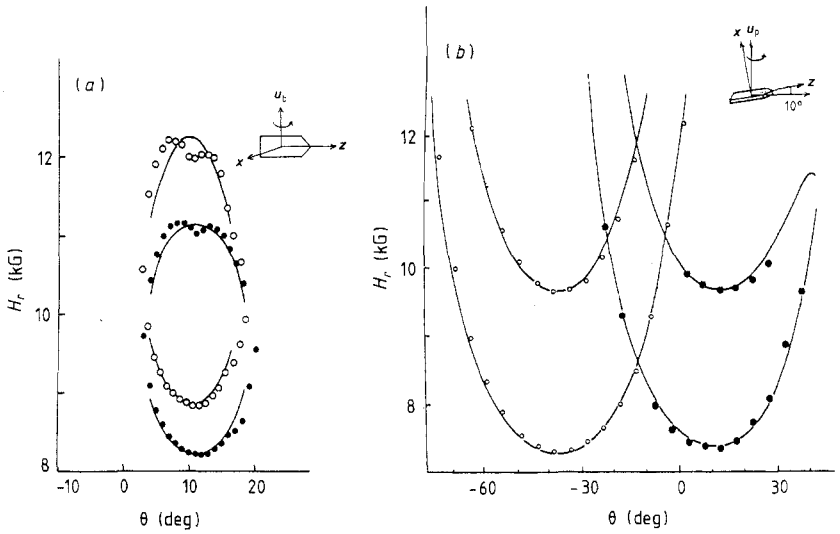

Figure 2. AFMR rotation patterns for $(DMCTTF)_2BF_4$. The orientations of the rotation axes are given in the insets (the shape of the crystal is schematic). (*a*) u_h and (*b*) u_p correspond respectively to the bubble-like and parabolic patterns. The continuous curves give the fits with the Nagamiya theory (the parameters are given in table 1).

For both phases the occurrence of two layers is revealed by the ESR signal, which presents two resonance lines for some positions of the magnetic field. These two lines can be separated at low temperature, enabling the separate study of each layer. For α-salts the behaviour of the two layers is identical, in agreement with the symmetry. Both layers exhibit a phase transition to an antiferromagnetic ground state at $T_N \simeq 20$ K. In the case of β-salts, the two lines behave independently and two different transition temperatures are found (as expected from the structure) both corresponding to an antiferromagnetic ordering. The assignment of each line to a particular layer can be made from the relative magnitude of the susceptibility. The conclusion is that the layer of type I has the highest Néel temperature $T_N \simeq 20$ K, while the strongly dimerised layer (type II) has a transition temperature approximately two times smaller, $T_N \simeq 10$ K.

The diagonalisation of the **g** tensor gives in both cases an estimate of the relative position of the molecular axes in each layer that is in rough agreement with the structures. However, this estimate is not accurate and will not be used for a complete orientation of the crystals for our discussion. Only the eigendirection for g_{min} is satisfactorily determined.

Other details concerning the physical properties in the paramagnetic phase will be found in paper A.

3. Antiferromagnetic resonance

Below the Néel temperature, one of the best experiments to probe the antiferromagnetic ordering is the antiferromagnetic resonance (AFMR). This technique has been successfully applied to various organic conductors using a standard X-band spectrometer (Coulon *et al* 1986a). In this case the experiment is made at fixed frequency and a search for resonances is made by rotating a crystal around various crystallographic axes. All

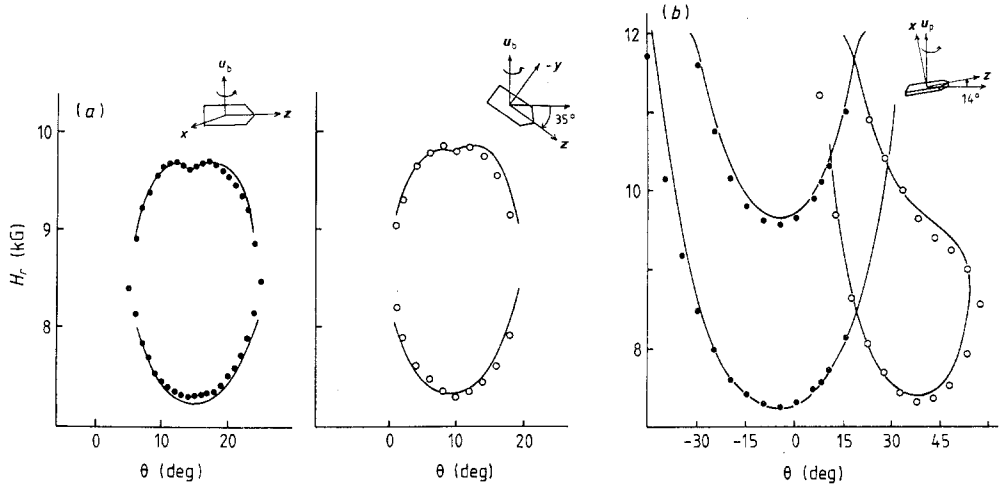

Figure 3. AFMR rotation patterns for α-(DMCTTF)$_2$ClO$_4$. The orientations of the rotation axes are given in inset (the shape of the crystal is schematic). (*a*) $\boldsymbol{u}_b$ and (*b*) $\boldsymbol{u}_P$ correspond respectively to the bubble-like and parabolic patterns. The continuous curves give the fits with the Nagamiya theory (the parameters are given in table 1).

our experiments were made at $T = 4.5$ K using the same cooling equipment as for ESR (Oxford Instruments ESR 900).

In the present study, the shape of the crystals is not simple, although they are thin plates. Thus the only direction which can easily be identified is the normal to the plates. Figures 2–5 summarise the experimental results. In every case, these figures correspond to the situation (Coulon *et al* 1986b) where $\omega_0 < \Omega_-$ and $\omega_0 < \Omega_{min} = (\Omega_+^2 - \Omega_-^2)^{1/2}$. To clarify the presentation we will separate the results for α- and β-salts.

3.1. Results for α-salts

Figures 2 and 3 give the rotation patterns obtained for (DMCTTF)$_2$BF$_4$ and α-(DMCTTF)$_2$ClO$_4$. The orientation of the crystal is given in the inset (the shape of the crystal is schematic). Two distinct sets of rotation patterns are found for both salts which should correspond to the two kinds of layers.

The bubble-like patterns indicate a rotation axis close to the *hard* axis, while figures 2(*b*) and 3(*b*) are characteristic of rotations around an axis close to *intermediate*. The slight asymmetry of the figures indicates that the rotation axes in the magnetic frame are not simple. Note that this asymmetry is more important in the case of the ClO$_4$ salt for one of the figures rotating around the axis labelled $\boldsymbol{u}_P$. As a consequence, the two bubbles cannot be observed rotating around the same axis as for the BF$_4$ salt. However, we will see that it is only small differences in the position of the magnetic axes that are responsible for this difference.

In both cases, the origin of the rotation is taken to be where the field is the closest from the largest dimension of the crystal in the plane of rotation. The correspondence between the two series of curves (open and filled symbols) is ensured by the existence of a common position of the magnetic field for the bubble-like and parabolic-like patterns. For example, $\theta = 10°$ in figure 2(*a*) is approximately the same orientation of the field as $\theta = 0°$ in figure 2(*b*).

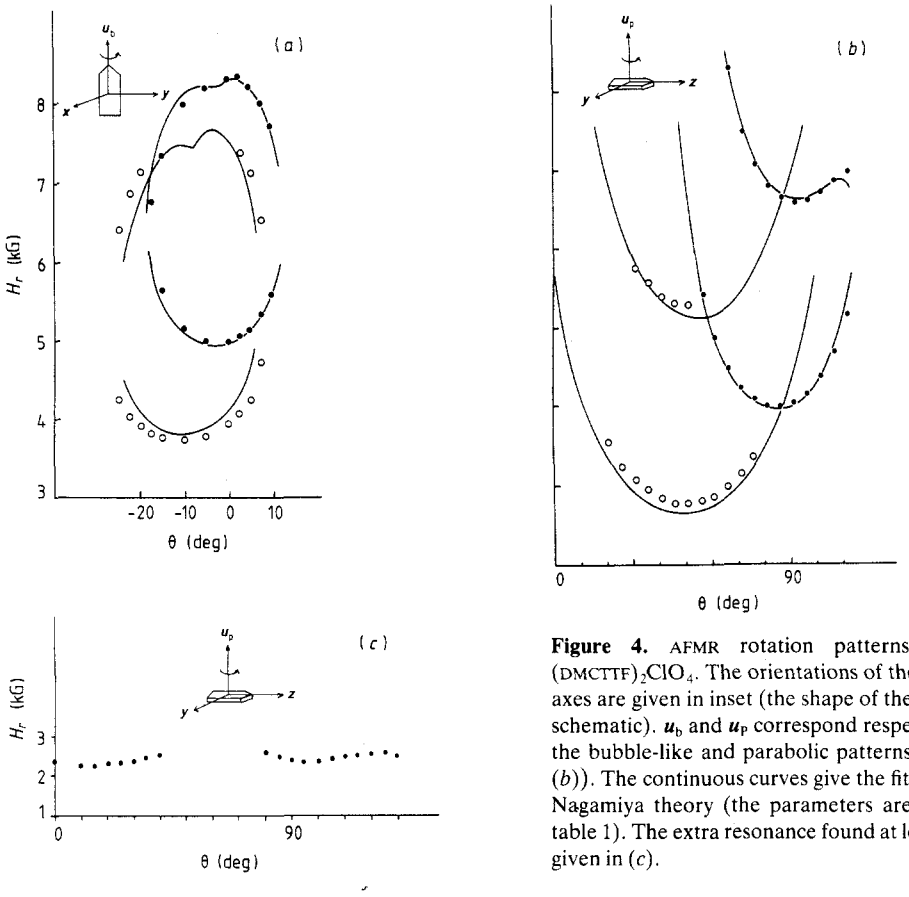

Figure 4. AFMR rotation patterns for β-(DMCTTF)$_2$ClO$_4$. The orientations of the rotation axes are given in inset (the shape of the crystal is schematic). $\boldsymbol{u}_b$ and $\boldsymbol{u}_p$ correspond respectively to the bubble-like and parabolic patterns ((*a*) and (*b*)). The continuous curves give the fits with the Nagamiya theory (the parameters are given in table 1). The extra resonance found at low field is given in (*c*).

The continuous lines give the fit of the data using the AFMR theory. This point will be discussed in the following section.

3.2. *Results for β-salts*

Figure 4 gives the AFMR results for β-(DMCTTF)$_2$ClO$_4$. As for the α-salts, the occurrence of two layers is revealed by the presence of two rotation patterns. In this case also we find either bubbles (when the rotation axis is along the largest dimension of the plates) or parabolic-like patterns (rotating the crystal around the normal to its plane). The origin of the rotation angle is defined as for the α-salts and the correspondence between the two series of figures is also easily obtained. In this case an extra resonance is found at low field when the rotation axis is the one of figure 4(*a*). This rotation pattern is given in figure 4(*c*). This mode is weakly sensitive to the field direction and has not been observed for other rotation axes.

The results for (DMCTTF)$_2$ReO$_4$ are closely related. However, only partial results were obtained in this case. They are given in figure 5. Only one parabolic-like pattern (figure 5(*a*)) has been obtained, with with a resonance field very close to one of the patterns shown by β-(DMCTTF)$_2$ClO$_4$. The other rotation pattern (figure 5(*b*)) is also reminiscent in part of the bubbles observed for the ClO$_4$ salt, as discussed in more detail

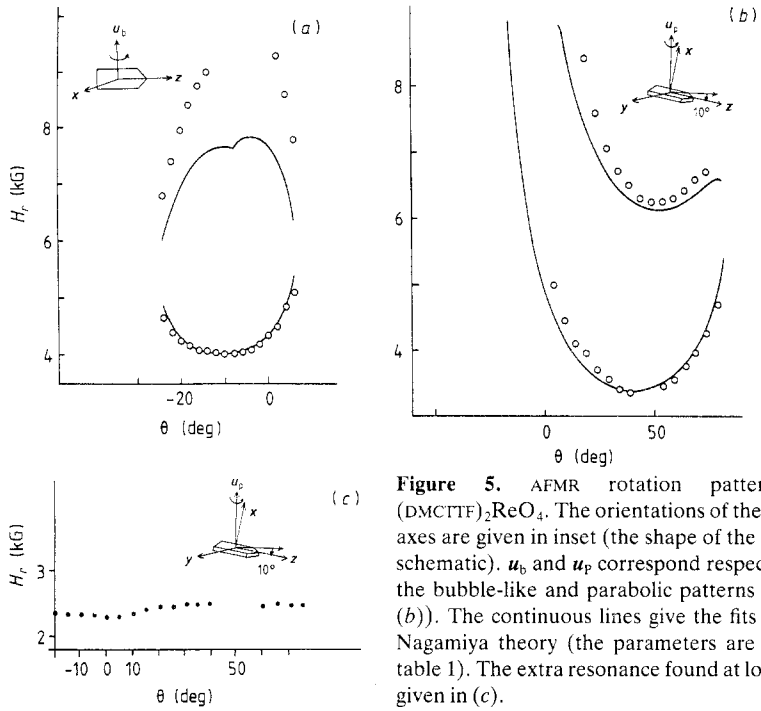

Figure 5. AFMR rotation patterns for $(DMCTTF)_2ReO_4$. The orientations of the rotation axes are given in inset (the shape of the crystal is schematic). u_b and u_p correspond respectively to the bubble-like and parabolic patterns ((*a*) and (*b*)). The continuous lines give the fits with the Nagamiya theory (the parameters are given in table 1). The extra resonance found at low field is given in (*c*).

in the last part of this paper. As for the ClO_4 salt, a resonance is found at low field when rotating around u_b (figure 5(*c*)).

The continuous curves also give the fits from the theory discussed below.

3.3. Fit of the data

The AFMR theory has already been successfully applied to many organic salts (Coulon *et al* 1986a). Since the experiments are made at low temperature (compared to T_N) the standard mean-field theory can be used (Nagamiya *et al* 1955). However, the situation is complicated in the present case since two differently oriented layers are found in the unit cell. Thus the coupling between these layers should be considered.

The exchange in the *c* direction is negligible and the only remaining interaction between the layers is due to dipolar forces. We have checked that the inter-layer contribution is weak and is only a small perturbation. Moreover, either for α- or β-salts the two layers have different molecular orientations and in both cases the corresponding AFMR modes are not degenerate (except for special positions of the magnetic field the frequencies of the mode of each layer are different). Thus we expect a small effect of the inter-layer interaction of the dynamic and we discuss below the behaviour of each layer ignoring this coupling (the discussion is thus similar to the one of samples with simple unit cells).

The fit with the Nagamiya theory gives for the rotation patterns of each layer the orientation of the rotation axes in the magnetic frame, together with the value of the three parameters: r, Ω_- and Ω_+. r accounts for some finite temperature effects ($r = 1$ at $T = 0, r = 0$ at $T = T_N$). The two other parameters are the zero-field frequencies (Coulon *et al* 1986b). Table 1(*a*) summarises the results. Since we have only partial results for the

Table 1. (*a*) AFMR parameters deduced from the fit, using the Nagamiya theory. Ω_- and Ω_+ are the zero-field frequencies, $r = (1 - \chi_{\parallel}/\chi_{\perp})$ where $\chi_{\parallel}$ and $\chi_{\perp}$ are the two components of the magnetic susceptibility. $\boldsymbol{u}_b$ and $\boldsymbol{u}_P$ are the rotation axes in the magnetic frame. (*b*) Deduced orientation of the magnetic axes relative to the crystal axes (defined in the insets of figures 2 to 5).

Anion		BF_4		α-ClO_4		β-ClO_4		ReO_4
(*a*)		II	II	II	II	I	II	II
	r	1		1		1	0.5	0.5
Ω_+	(kG)	13.8		13.6		10	9.5	9.6
Ω_-	(kG)	9.0		9.0		7	4.5	4.4
	(deg)							
$\boldsymbol{u}_b$	θ	21	26	2	15	15	30	30
	ϕ	177	−7	5	60	205	30	30
$\boldsymbol{u}_P$	θ	85	89	90	70	80	87	87
	ϕ	94	89	90	−84	99	102	102

		α-(DMCTTF)$_2ClO_4$		β-(DMCTTF)$_2ClO_4$	
(*b*)	(deg)	II	II	I	II
$\boldsymbol{E}$	θ	15	45	90	50
	ϕ	180	−104	−90	−100
$\boldsymbol{I}$	θ	75	75	75	75
	ϕ	0	0	0	0
$\boldsymbol{H}$	θ	90	48	15	40
	ϕ	90	104	180	90

ReO_4 salt, we have simply checked that the rotation axes previously obtained for β-ClO_4 (for the corresponding layer) give reasonable fits with similar values of r, Ω_- and Ω_+. Finally, in the case of β-salts the assignment of the layers is possible from the value of r: the smaller T_N, the smaller r. Thus, the layer of type II should correspond to $r = 0.5$, while $r = 1$ is related to the layer of type I.

The next step is to determine by inversion the position of the magnetic axes with reference to the crystal axes. The results for both ClO_4 phases are given in table 1(*b*). Round numbers have been given, taking account of the accuracy of this determination. The result for the BF_4 salt is very similar to the one for α-ClO_4. The difference observed between figures 2 and 3 arises from a different crystal orientation in the experiments. The partial result for the ReO_4 salt also mimics the β-ClO_4 behaviour.

In summary, within each group (α or β) the orientation of the magnetic axes (and the corresponding eigenvalues following table 1(*a*)) are very similar. For this reason, we essentially consider the data of the ClO_4 salts for the discussion of the anisotropy in § 5.

4. Transfer integrals

The electronic band structures of organic conductors have been determined by theoretical models showing several degrees of sophistication (Grant 1983a, Minot and Louie 1982). The self-consistent *ab initio* band structure of β-(BEDT-TTF)$_2I_3$ was recently

Table 2. Calculated transfer integrals (defined in figure 1). (*a*) for layers of type I; (*b*) for layers of type II.

(*a*)	*X*	t_{S1}	t_{S2}	t_{I1}	t_{I2}	t_{I3}
	β-ClO_4	141.7	77.2	15.3	17.7	−3.2
	AsF_6	160.6	76.7	14.4	19.0	−5.3

(*b*)	*X*	t_{S1}	t_{S2}	t_{I1}	t_{I1}'	t_{I2}	t_{I3}
	β-ClO_4	148.8	46.4	3.3	1.8	−30.8	−18.8
	α-ClO_4	169.6	36.5	6.1	1.8	0.6	−19.4
	BF_4	165.6	37.7	7.5	2.0	−2.9	−21.9

performed (Kubler *et al* 1987), but this type of calculation requires a very large amount of computational time which limits its application. For a series of salts based on the same organic molecule, the use of a semi-empirical method is appropriate since it is expected that the general trends and differences will appear from the comparison of closely related compounds. Thus, various semi-empirical calculations, mostly based on the extended Hückel (EHT) formalism, were performed in the last few years (Grant 1983a, Minot and Louie 1982, Mori *et al* 1985, Ducasse *et al* 1986). We use the same technique for the present work.

The transfer integrals involve the coupling between the HOMO (highest occupied molecular orbital) of each organic molecule. This HOMO has a Π character built on the p_z atomic orbitals of the carbon and chalcogenide atoms (the *z* axis is taken perpendicular to the mean molecular plane). The transfer integrals are then evaluated using the dimer splitting approximation $t = \langle \mathrm{HOMO}_1 | H | \mathrm{HOMO}_2 \rangle$ where H is the effective extended Hückel Hamiltonian.

Transfer integrals were calculated for the 300 K crystal structures of the $(\mathrm{DMCTTF})_2\mathrm{X}$ salts using the parameters defined in a recent work on Bechgaard salts (Ducasse *et al* 1986). This choice has proved convenient, as the theoretical nesting vector determined from the refined band structure of $(\mathrm{TMTSF})_2\mathrm{PF}_6$ is in good agreement with the experimental value of the spin-density wavevector derived from the NMR investigations (Delrieu *et al* 1986, Takahashi *et al* 1986).

The labelling is depicted in figure 1. The same notation can be used for both types of layers (weakly or strongly dimerised). However, for layers of type II an extra transfer integral t_{I1}' has to be considered. As we will see in the discussion this interaction competes with t_{I1}.

The layers of type I are organised in chains: t_{S1} and t_{S2} are the intra-chain interactions while the t_{Ii} are inter-chain transfer integrals. For example, t_{I3} labels the interaction between monomers translated by $\boldsymbol{b}$ (or $\boldsymbol{a}$). In contrast, the layers of type II are organised in dimers: t_{S1} is the intra-dimer interaction, while the other transfer integrals describe the inter-dimer interactions in the layer. In both cases, the inter-layer interaction is negligible in the $\boldsymbol{c}$ direction, as it was for the TMTSeF salts (Grant 1983b). The transfer integrals calculated are listed in tables 2(*a*) and 2(*b*) for layers of type I and II respectively. For comparison, the result for $(\mathrm{DMCTTF})_2\mathrm{AsF}_6$, which presents weakly dimerised chains, is also given.

For the two compounds of type I, the sets of integrals are very similar. The intra-stack interactions t_{S1} and t_{S2} are larger than the inter-chain integrals t_{Ii}, illustrating the

quasi-one-dimensionality of these systems. The ratio t_{S1}/t_{S2} close to two indicates a noticeable dimerisation of the chains. Finally, as already observed in the TMTTF and DMTTF compounds, the inter-chain interactions can be positive or negative, depending on the relative position of two neighbouring stacks. The consequence of this finding will be analysed below.

Layers of type II have a much more two-dimensional structure. Although t_{S1} is almost the same as previously, t_{S2} has a smaller value, which is now similar to some of the t_{1i} integrals. Some differences appear between α- and β-salts, as evidenced from the value of t_{12}, large and negative for β-ClO_4 but small for the α-salts. This latter value results from the following observation. The shift along the short axis of one molecule with respect to the other is almost equal to half the molecular width, while the shift along the long axis is roughly equal to the C–C bond length. This special situation implies a very small overlap. In the case of β-ClO_4, the shift along the short axis is larger by about 40% than the molecular width and the resulting integral is large and negative.

5. Discussion

We discuss in this section the interactions in the antiferromagnetic phase to explain the AFMR results. For clarity we will analyse layers of type I and II separately.

5.1. Exchange interactions

5.1.1. Layers of type I. These layers are organised into chains. This type of structure has already been found for the extensively discussed TMTTF and TMTSF salts. Following these theories, electronic localisation originates from electron correlations and from the dimerised structure of the chains (Bourbonnais 1986, Bourbonnais and Caron 1987). The relevance of Umklapp terms implies the existence of the minimum of resistivity at T_ρ below which an activated resistance is found. At the same time, 1D AF fluctuations are present.

Within the same description, the antiferromagnetic ground state is stabilised, thanks to the occurrence of finite inter-chain couplings. When the electronic localisation is present, the relevant mechanism is called IEX (interchain exchange coupling). The corresponding inter-chain exchange is optimum for a wavevector with a $\boldsymbol{b}$ component which reads (Caron and Bourbonnais 1988) $q_b = (\pi/b)(1 + 2\Phi/\pi)$ where Φ is a parameter function of the transfer integrals between neighbouring molecules.

The same wavevector optimises the nesting of the Fermi surface and the expression of Φ can be found in papers devoted to band-structure calculations (Ducasse *et al* 1985). The recent theory of Caron and Bourbonnais rationalises the importance of Φ already mentioned empirically (Ducasse *et al* 1985) even when the Fermi surface is not relevant (i.e. in the localised regime).

The parameter Φ is extremely sensitive to details of the structure and thus is temperature-dependent. As a consequence, low temperature structures are necessary to obtain its value at the Néel temperature. These data are still missing for the DMCTTF salts, limiting the discussion on layers of type I.

5.1.2. Layers of type II. In this case all the inter-dimer transfer integrals are small compared with electron–electron interactions. Therefore the strong-coupling limit is appropriate. In this description, the kinetic part of the Hamiltonian is considered as a perturbation. Up to second order, it generates exchange integrals between the dimers.

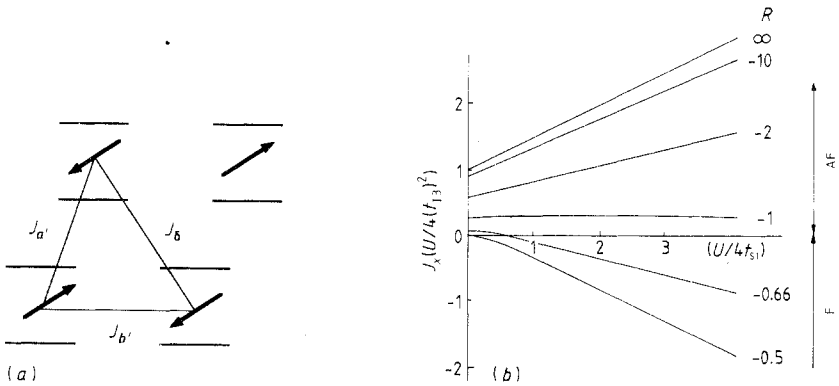

Figure 6. (*a*) Definition of the three relevant exchange couplings. The magnetic superstructure found for α- and β-salts is also shown. (*b*) Normalised exchange coupling in the ***b*** direction for different values of $R = t_{13}/(t_{11} - t'_{11})$ as a function of $U/4t_{S1}$. The exchange is taken positive for an antiferromagnetic coupling.

This is supported by the temperature-dependence of the spin susceptibility in the paramagnetic phase, which is characteristic of a spin lattice (see paper A).

As shown in figure 6(*a*), three energies should be considered (the relation between ***a'***, ***b'*** and ***δ*** depends on the material). In the ***a'*** and ***δ*** directions the exchange is antiferromagnetic and simply proportional to the square of the corresponding transfer signal (Pincus 1972). In the ***b'*** direction, several transfer integrals are in competition. The resulting exchange is either ferro or antiferromagnetic (Laversanne *et al* 1986). In our case t_{13} is large and negative while t_{11} and t'_{11} are small. The introduction of t'_{11} is straightforward in the calculation.

Figure 6(*b*) gives the dependence of $J_{b'}$ on U (normalised by the intra-dimer transfer integral) for different values of $R = t_{13}/(t_{11} - t'_{11})$. Moreover, from the results given in table 2(*b*), the three exchange interactions can be estimated. Taking $U \approx 1$ eV, the largest exchange is in both cases of the order of 30 K. The relative magnitude of the three terms $J_{a'}$, $J_{b'}$ and J_δ is 1 : 1 : 0 for α-salts, 1 : 1 : 0.5 for β-salts. Therefore the expected superstructure is $(2a', 2b')$ in both cases. In agreement with experiment, we also predict a higher T_N for α-salts than for β-salts, since in the latter case J_δ comes in opposition to the two other terms. For example, at the mean-field approximation, one obtains $T_N \simeq 2(J_{a'} + J_{b'} - J_\delta)$ which gives $T_N^\beta / T_N^\alpha \simeq 0.75$. Obviously, the introduction of fluctuations is necessary for a more quantitative comparison with experiment.

5.2. *Magnetic anisotropy*

Although very small, the magnetic anisotropy is essential to describe the AF ground state either for weakly or strongly dimerised samples (Roger *et al* 1986, Laversanne *et al* 1986). In both cases the anisotropy is essentially due to dipolar interactions, but the description is different according to the nature of the layer.

The layers of type I, the anisotropy tensor has been determined by considering a sinusoidal distribution of the spin on the chains (Roger *et al* 1986). A relation is found between the anisotropy and the parameter Φ defined previously. In particular, a clear correlation is found between Φ and the position of the magnetic axes. We profit from this relation in the following.

Table 3. Calculated orientation of the magnetic axes relative to the molecular axes. θ and ϕ are the spherical coordinates of these axes. W_{EI} and W_{EH} are the corresponding anisotropy energies (defined in the text).

Sample	Easy axis (deg) θ	Easy axis (deg) ϕ	Intermediate axis (deg) θ	Intermediate axis (deg) ϕ	Hard axis (deg) θ	Hard axis (deg) ϕ	W_{EI} (mK)	W_{EH} (mK)
$(DMCTTF)_2BF_4$	24	135	82	26	112	113	2.1	6.7
α-$(DMCTTF)_2ClO_4$	25	134	81	26	113	112	2.0	6.6
β-$(DMCTTF)_2ClO_4$	21	125	87	27	111	116	2.1	6.6

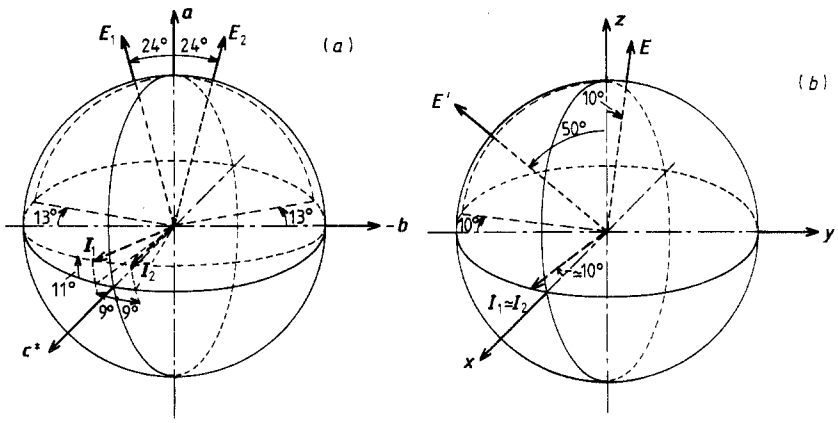

Figure 7. α-salts: (*a*) Calculated result: position of the magnetic axes of both layers of type II in the crystallographic frame (c^*, $-b$, a). E and I stand for easy and intermediate axes. The indices 1 and 2 correspond respectively to the layer located at the origin and at $c/2$ in the unit cell given in paper A. (*b*) Experimental result: position of the magnetic axes relative to the crystal axes (x, y, z) defined in inset of figures 2 to 5.

For samples of type II, the anisotropy has been estimated for several salts, assuming one spin localised per dimer (Laversanne *et al* 1986). We use the same technique to estimate the anisotropy of our samples. The essential difference is a different magnetic superstructure.

5.2.1. α-salts. In this case, both layers are of type II and are related by symmetry. We have calculated the anisotropy for one of these layers (the layer located at the origin following the figure 2(*a*) of paper A). As previously mentioned, the inter-layer interaction is weak and we have made a 2D calculation considering only the interactions inside the layer. The results are given in table 3. They are similar for the BF_4 and α-ClO_4 salts. One important point is that we find the easy axis close to g_{min}. This is clearly the consequence of the magnetic superstructure, which favours the orientation of the spins in a direction close to the normal of the molecules. The intermediate and hard axes are respectively close to g_{max} and g_{int}. The magnetic frame of the other layer is then deduced by symmetry. Finally, using structural data, we have deduced the position of the magnetic axes in the crystallographic frame (c^*, $-b$, a). Figure 7(*a*) summarises this calculation.

The comparison with experiments requires more information on the orientation of the crystals (i.e. the relation between the x, y, z axes shown in inset of figures 3 and 4 and the crystallographic axes). In previous studies, this orientation has been done from the diagonalisation of the **g** factor. In the present case, this method is not accurate because of the presence of two lines (see paper A) and we had to proceed differently.

Quite generally, the axis perpendicular to the plane of the crystals is c^* (Sugano *et al* 1986) and we have assumed that it is also the case for our crystals. This is in agreement with the information deduced from the **g** factor. With this assumption, the plane of the crystals (yz) is also the (ab) plane.

The comparison between the calculation and the fit of AFMR data is illustrated by figure 7. The agreement with the calculation is shown by:

(i) the orientation of the easy axes, which are at about 10° from the (ab) plane with an angle between them of about 50°,

(ii) the position of the intermediate axes close to c^*, with a small angle between them (of about 10°).

This comparison also indicates that z is at about 25° from a. Further structural data are necessary to confirm this analysis.

The calculation also gives the anisotropy energies W_{EI} and W_{EH} (see table 3). We find the same order of magnitude as for other strongly dimerised salts (Laversanne *et al* 1986). The comparison with the experiment is straightforward. The ratio W_{EH}/W_{EI} is simply related to the zero-field frequencies through $W_{EH}/W_{EI} = (\Omega_+/\Omega_-)^2$. The ratio obtained from the 2D calculation is 3.3, higher than the experimental result of 2.4. The agreement can be improved by considering the interlayer interaction (Vaca 1988). Considering the two possible commensurate superstructures in the c direction, the previous ratios become respectively 2.7 and 4. The former result corresponds to the situation with the lowest interlayer dipole–dipole interaction and is clearly the one which improves the agreement between theory and experiment (from table 1(a), the experimental ratio is 2.3). This suggests that the anisotropy interaction may be relevant to determine the superstructure in the c direction. At the same time, the position of the magnetic axes is not noticeably changed by the inter-layer coupling and the discussion previously given from the 2D calculation is correct.

5.2.2. β-salts. In this case each type of layer is present in the structure. As already mentioned, knowledge of the low temperature value of Φ is necessary to estimate the magnetic anisotropy of weakly dimerised layers. This information is still missing in our case and so a direct discussion for the layers of type I is impossible.

Considering the strongly dimerised layers, we have also estimated the anisotropy with a 2D calculation. The results are given in table 3 for β-ClO_4. They are very close to the ones for α-salts. This is not surprising since the magnetic superstructure is the same while the anisotropy tensor is not strongly dependent on small details of the structure (Laversanne 1987).

As in the previous case, the orientation of the crystal cannot be deduced from the **g** factor. With similar arguments, we assume that c^* is perpendicular to the plane of the crystal. This is in agreement with the results given in table 1(b) which give a similar orientation of the intermediate axis close to the normal to the crystals. Contrary to the situation for α-salts, no argument based on the symmetry can be used for a further orientation in the (yz) plane. The only partial result obtained from the **g** factor is an

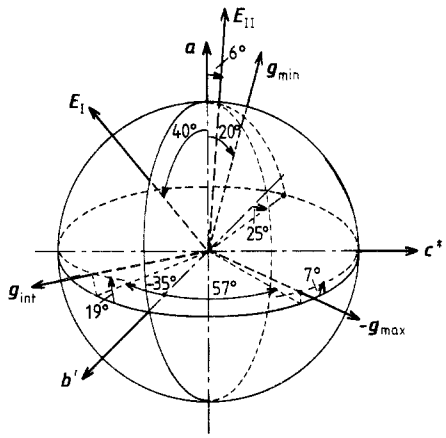

Figure 8. β-salts: Position of the magnetic axes of both layers in the crystallographic frame (c^*, $-b$, a). The magnetic axes of the strongly dimerised layer (type II) are located from the calculation and the magnetic frame of the other layer (type I) is then deduced from the experiment.

angle of about 20° between the easy axis of the layer of type II and g_{min}, which is in agreement with the calculation (see table 3).

To extract more information from our data, we have assumed a perfect agreement between the calculation and the experiment for the layer of type II. Then we can use the experimental result (table 1(b)) for the orientation of the (x, y, z) axes in the crystallographic frame. It becomes straightforward to deduce the position of the magnetic axes of the weakly dimerised layer (type I) relative to these axes. The result is given in figure 8. In particular we deduce that the corresponding easy axis E_I makes an angle $\theta_E \approx 40°$ with a. Following the result of Roger *et al*, this implies a value of Φ (defined previously) close to 90°. Although the calculation of Roger *et al* was made for a TMTTF salt, it should also roughly apply in the present case since the anisotropy is only weakly dependent on the details of the structure.

This result is important in discussing the nature of the low temperature magnetic ground state. It has been recently argued that Φ close to 90° favours an antiferromagnetic ground state (Coulon *et al* 1988, Vaca 1988). The present result is in agreement with these conclusions.

The eigenvalues of the anisotropy are also given in table 3. The result of the 2D calculation is similar to the one for α-salts and the corresponding ratio W_{EH}/W_{EI} is also 3.3. As previously, this estimate can be improved by considering the inter-layer coupling. To obtain an estimate of this correction, we have assumed one spin localised per dimer for the weakly dimerised layer (a more sophisticated spin distribution would be necessary for an accurate estimate). We get the same order of magnitude of the correction as for α-salts. Considering the two possible commensurate superstructures in the c direction, the ratio W_{EH}/W_{EI} becomes 2.9 and 3.4 respectively. The latter value is closer to the experimental value, which is 4.5, indicating that inter-layer contributions to the anisotropy are not negligible for deducing the anisotropy energy. As in the previous case, the correction to the position of the magnetic axes is negligible.

6. Summary

In summary, we have discussed the antiferromagnetic properties of DMCTTF salts with tetrahedral anions, starting with transfer-integral calculations and AFMR results. The originality of these compounds is in the occurrence of two organic layers in the unit cell

and the presence of two different phases according to the size of the anion. In the case of α-salts, the two layers are symmetry-related. We find the same AF parameters for both layers, only with a different orientation of the magnetic axes. For β-salts, the layers are independent. Different magnetic interactions and different orientations of the magnetic axes are found. For both kinds of samples, the inter-layer coupling is weak and the magnetic interactions can be discussed using a 2D description. For strongly localised layers, we have discussed the exchange and anisotropy from the room-temperature structure. The calculation of the anisotropy agrees with the experiment and confirms the analysis previously done for other samples of type II.

Layers of type I should be discussed with the low temperature structure, since the Φ parameter, which determines the magnetic superstructure, is T-dependent. Since these data are still missing, we have used our determination of the magnetic axes to deduce Φ at low temperature. We find a value in agreement with the occurrence of a magnetic ordering (i.e. close to 90°). Further structural data would be useful to confirm this result.

References

Bourbonnais C 1986 *Proc. NATO Advanced Study Institute in Low Dimensional Conductors and Superconductors* ed. D Jerome and L G Caron (New York: Plenum) 155

Bourbonnais C and Caron L G 1987 *Synthetic Metals* **19** 333

Caron L G and Bourbonnais C 1988 *Proc. ICM 88 (Paris)* at press

Coulon C, Laversanne R and Amiell J 1986a *Physica* B **143** 425

Coulon C, Scott J C and Laversanne R 1986b *Phys. Rev.* B **33** 6235

Coulon C, Vaca P, Granier T and Gallois B 1988 *Synth. Met.* **27** B 449

Delrieu J M, Roger M, Toffano Z, Moradpour A and Bechgaard K 1986 *J. Physique (Paris)* **47** 839

Ducasse L, Abderrabba A and Gallois B 1985 *J. Phys. C: Solid State Phys.* **18** L947

Ducasse L, Abderrabba A, Hoarau J, Pesquer M, Gallois B and Gaultier J 1986 *J. Phys. C: Solid State Phys.* **19** 3805

Giral L, Faber J M and Gouasmia A 1986 *Tetrahedron Lett.* **27** 4315

Granier T and Gallois B 1989 unpublished

Grant P 1983a *J. Physique Coll.* **44** C3 847

—— 1983b *J. Physique Coll.* **44** C3 1121

Kubler J, Weger M and Sommers C B 1987 *Solid State Commun.* **62** 801

Laversanne R 1987 *PhD Thesis* University of Bordeaux, France

Laversanne R, Coulon C, Amiell J and Morand J P 1986 *Europhys. Lett.* **2** 401

Minot C and Louie S G 1982 *Phys. Rev.* B **26** 4793

Mori T, Kobayashi A, Sasaki Y, Kato R and Kobayashi H 1985 *Solid State Commun.* **53** 627

Nagamiya T, Yosida K and Kubo R 1955 *Adv. Phys.* **4** 1

Pincus P 1972 *Solid State Commun.* **11** 305

Roger M, Delrieu J M and Wope Mbougue E 1986 *Phys. Rev.* B **34** 4952

Sugano T, Saigo G and Kinoshita M 1986 *Phys. Rev.* B **34** 117

Takahashi T, Maniva Y, Kawamura H and Saito G 1986 *J. Phys. Soc. Japan* **55** 1364

Vaca P 1988 *PhD Thesis* University of Grenoble, France

Vaca P, Granier T, Gallois B, Coulon C, Gouasmia A K and Fabre J M 1988 *J. Phys. C: Solid State Phys.* **21** 5719